

The efficiency of mixing in sheared, stratified turbulence: inferences from direct simulations and oceanographic observations

W.D. Smyth, J.N. Moum and D.R. Caldwell
College of Oceanic and Atmospheric Sciences
Oregon State University, Corvallis OR 97331-5503
smyth@oce.orst.edu, moum@oce.orst.edu, caldwell@oce.orst.edu

1. Abstract

We investigate the time evolution of mixing in turbulent overturns, using a combination of direct numerical simulations (DNS) and microstructure profiles obtained during two field experiments. Our focus is on the flux coefficient Γ , the ratio of the rate of working against gravity by turbulence to the kinetic energy dissipation rate ϵ . In observational oceanography, a constant value $\Gamma = 0.2$ is often used to infer the buoyancy flux and the turbulent diffusivity from measured ϵ . Both simulations and observations indicate that Γ varies systematically in time, decreasing by an order of magnitude or more over the life of a turbulent overturn. The results suggest useful parameterizations for both Γ and turbulence age in terms of the ratio of Ozmidov scale to Thorpe scale.

2. Introduction

In this paper, we investigate the efficiency of mixing by turbulent overturns in the ocean thermocline. In particular, we are interested in variations of the flux coefficient, Γ , in time over the life cycle of a turbulent event. (The flux coefficient is closely related to mixing efficiency: it is the ratio of work done against gravity to energy dissipated via friction.) Our approach employs a combination of microstructure observations and direct numerical simulations.

In oceanic applications, Γ is often treated as a constant, usually with the value 0.2, and used to estimate heat and salt fluxes from measurements of the kinetic energy dissipation rate, ϵ (e.g. Smyth et al., 1996). However, an accumulation of observational evidence suggests that Γ is, in fact, significantly variable (Garrett and Moum, 1995; Moum, 1996a; Ruddick et al., 1997). Here, we investigate the possibility that Γ evolves systematically in time as turbulent overturns grow, break and decay.

We investigate the time-dependence of Γ using two very different approaches: direct numerical simulations (DNS) and field observations of turbulent microstructure. These two methods were chosen because their respective strengths and weaknesses are complementary. The time dependence of Γ is easy to assess in DNS output, but the validity of DNS as a model of ocean turbulence is limited to low Reynolds number and specified initial and boundary conditions. In contrast, microstructure measurements sample genuine ocean turbulence, but neither Γ nor time (relative to onset) can be measured directly. These limitations of the observational data can be circumvented by means of two assumptions:

1. The ratio of the Ozmidov to the Thorpe length scale, $R_{OT} = L_O/L_T$, varies monotonically in time and can therefore be used to indicate the evolutionary stage of an observed overturn (e.g. Wijesekera and Dillon, 1997).
2. Γ can be approximated by $\Gamma_d = \kappa CN^2/\epsilon$, where κ is the scalar diffusivity, C is the Cox number (to be defined later) and N is the Brunt-Vaisala frequency (Osborn and Cox, 1972; Oakey, 1982).

Insofar as assumptions (1) and (2) are valid, the time dependence of Γ can be assessed using observational data. Here, DNS results will be used to examine the time dependence of Γ directly, and also to test assumptions (1) and (2) above. Having established the range of validity of these assumptions, we then proceed to examine the relationship between Γ_d and R_{OT} in the observational data.

DNS and observational methods are described in section 3. In section 4, we describe mixing in the simulated flows. Preturbulent overturns are shown to mix very efficiently, to the extent that a substantial fraction of the net mixing occurs before the onset of turbulence. As turbulence begins to decay, the flux coefficient asymptotes to 0.2. We then ask whether or not the same behaviour is evident in oceanic observations. In sections 5 and 6, we assess the validity of the two assumptions (described above) needed for the interpretation of the observational results. The observed evolution of the flux coefficient is then described in section 7. The results confirm that the flux coefficient decreases dramatically as turbulence evolves. Section 8 summarizes our conclusions.

3. Methodology

3.1 Direct numerical simulations of breaking Kelvin-Helmholtz billows

Our simulations are done in a domain with periodic boundary conditions in the two horizontal dimensions and zero flux conditions at the upper and lower boundaries. The full Navier-Stokes equations are solved, with buoyancy effects represented via the Boussinesq approximation. Spatial derivatives are evaluated using Fourier transforms in the horizontal dimensions, second-order centered differences in the vertical. Time advancement is via a second-order Adams-Bashforth method. Each simulation is initialized with a parallel flow in which shear and stratification are concentrated a horizontal layer surrounding the plane $z = 0$:

$$\tilde{u}(z) = \frac{u_o}{2} \tanh \frac{2z}{h_o}; \quad \tilde{\theta}(z) = \frac{\theta_o}{2} \tanh \frac{2z}{h_o}, \quad (1)$$

plus a small perturbation to initiate instability. The flow develops a train of Kelvin-Helmholtz billows which subsequently merge and break down into turbulence via a sequence of secondary instabilities. The dimensions of the computational domain are chosen on the basis of linear stability analysis to accommodate two wavelengths of both the primary and the secondary instability.

The constants defining the initial conditions (1) can be combined with the kinematic viscosity $\nu = 1.0 \times 10^{-6} m^2 s^{-1}$, the gravitational acceleration $g = 9.8 m s^{-2}$ and the diffusivity κ to form three dimensionless groups whose values determine the stability of the flow at $t = 0$: the initial Reynolds number $Re \equiv u_o h_o / \nu$, the initial bulk Richardson number $Ri_o \equiv g \theta_o h_o / u_o^2$, and the Prandtl number $Pr \equiv \nu / \kappa$. Values of these parameters are given in table 1.

Extensive comparison with oceanographic measurements has shown that, while Reynolds numbers achieved in the simulations are at the small end of the observed range, most other turbulence statistics tested are consistent with observations (Smyth et al., 2000). These include measures of large eddy geometry, as well as statistics relating background stratification, kinetic energy, and dissipation rates. We conclude that our simulated overturns provide an acceptable model for turbulent events in the thermocline. Further information is given in Smyth (1999) and Smyth and Moum (2000b).

3.2 Observations of turbulent overturns in the ocean thermocline

Two observational datasets are used in the present study. The first was collected during the FLUX STATS experiment (FLX91) in May 1991 off the coast of northern California. Measurements made by the free-falling profiler Chameleon included pressure (depth), temperature, conductivity, temperature-gradient fluctuations using an FP07 microbead thermistor, horizontal velocity-gradient fluctuations using airfoil shear probes, and vertical velocity fluctuations using a Pitot tube (Hebert and Moum, 1994; Moum, 1996a,b). From 400 profiles, 3425 overturns were selected using principles similar to those of Moum (1996b). A second set of 1155 events was selected from the Tropical Instability Wave Experiment (TIWE), conducted at the equator at 140°W in December 1991 (Lien et al., 1995). The overturns were all located in the upper thermocline between 60 and 200m depth, and spanned both the upper and lower flanks of the Equatorial Undercurrent.

Simulation	Pr	Re_o	L_x (m)	L_y (m)	L_z (m)	Δx (10^{-2} m)	h_o (m)	u_o (10^{-3} m/s)	θ_o (10^{-6} K)	Symbol
1	7	1354	2.73	0.34	1.36	0.53	0.20	8.34	2.00	•
2	4	1967	3.29	0.41	1.63	0.64	0.24	10.00	2.41	*
3	1	4978	5.24	0.65	2.62	1.03	0.38	13.27	3.83	○

Table 1: Parameter values describing a sequence of three simulations of breaking Kelvin-Helmholtz billows. L_x, L_y and L_z are the domain dimensions, and $\Delta x (= \Delta y = \Delta z)$ is the grid interval. Initial conditions are characterized by the length scale h_o , the velocity scale u_o and the temperature scale θ_o . Pr is the Prandtl number; Re_o the initial Reynolds numbers. For all simulations, the initial bulk Richardson number was $Ri_o = 0.08$. All simulations described here employed array sizes of $512 \times 64 \times 256$.

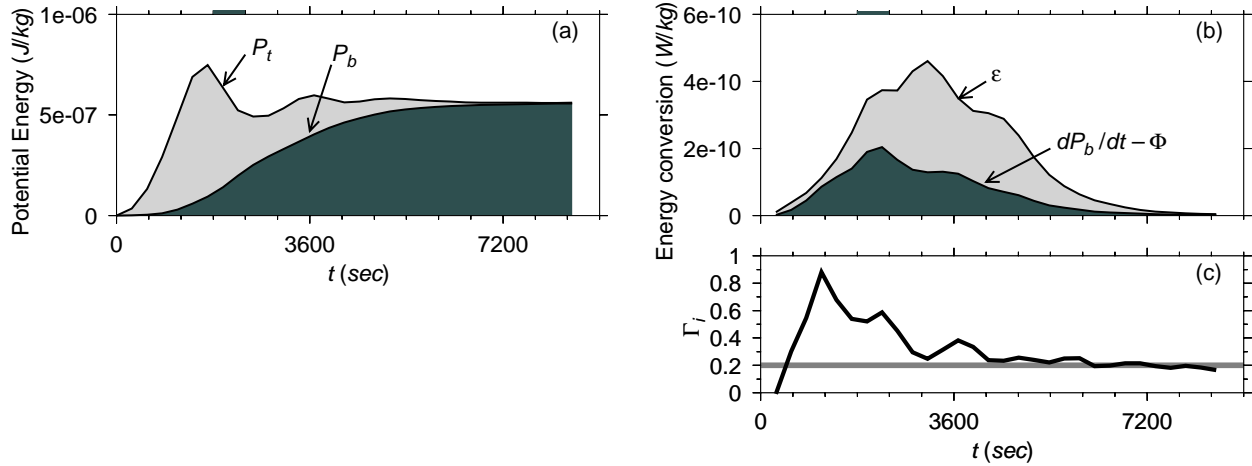


Figure 1: Evolution of various quantities describing work done against gravity for the $Pr = 7$ simulation. (a) The upper (lower) curve denotes the total (background) potential energy. Shaded bars at the tops of (a) and (b) mark the approximate time of the onset of turbulence. (b) Volume-averaged perturbation kinetic energy dissipation rate (upper curve) and rate of irreversible potential energy increase due to fluid motions (lower curve). The latter is dP_b/dt minus Φ , the rate of potential energy increase that would occur in a state of rest. The ratio of the lower to the upper ordinate is Γ_i . (c) Γ_i .

4. Flux coefficient evolution in simulated flows

In figure 1, we show various aspects of potential energy evolution for the case $Pr = 7$. The total potential energy is denoted as P_t , while P_b indicates the background potential energy, i.e. the minimum potential energy achievable via reordering of the density field (Winters et al., 1995). The difference $P_t - P_b$ is the available potential energy. Early in the simulation, most of the work done against gravity is reversible, i.e. it contributes to the available potential energy (figure 1a). The latter grows to a maximum near $t = 1600s$, then decreases rapidly (i.e. the wave breaks). The background potential energy grows monotonically and, ultimately, becomes equal to the total potential energy as vertical motions decay.

In figure 1b, we see that the rate of irreversible work done against gravity peaks quite early in the simulation; in fact, it peaks as the billow is breaking. The dissipation of kinetic energy, in contrast, peaks near $t = 3000s$, after the transition to turbulence is complete. This offset between maximum irreversible work and maximum kinetic energy dissipation leads to large values of the instantaneous flux coefficient, $\Gamma_i = (dP_b/dt - \Phi)/\epsilon$, early in the simulation (figure 1c). This highly efficient mixing occurs in the braids connecting adjacent Kelvin-Helmholtz billows. After the onset of turbulence, Γ_i decreases and appears to asymptote to the canonical value 0.2.

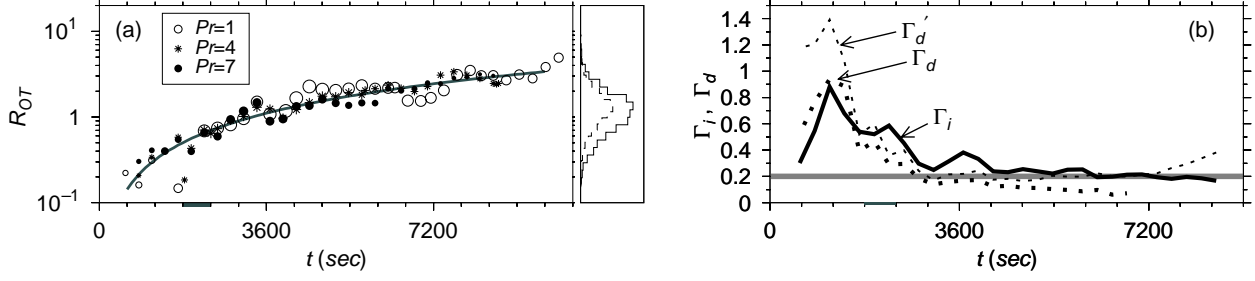


Figure 2: (a) Evolution of the ratio of the Ozmidov scale to the Thorpe scale. At selected times during each simulation, 512 vertical profiles were taken through the simulated flowfields and analyzed as if they were microstructure profiles (Moum, 1996b; Smyth et al., 2000). Each plotted symbol represents the median of R_{OT} obtained from a particular simulation at a particular time. The shaded bar at the top marks the approximate location of the transition to turbulence. The solid curve represents (2). The histograms at the right represent the probability distributions of R_{OT} in the two observational datasets: TIWE (solid) and FLX91 (dashed). (b) Comparison of the instantaneous flux coefficient Γ_i and its approximation Γ_d for simulation 1. Thick, solid curves: Γ_i . Thin dashed curves: Γ'_d , computed using the unaltered ϵ field. Thick dashed curves: Γ_d computed after applying noise field and ϵ threshold to DNS profiles. The horizontal line indicates the standard value 0.2. Shaded bars mark the approximate time of the transition to turbulence.

5. R_{OT} as an indicator of turbulence age

In figure 2a, we demonstrate that R_{OT} represents an effective clock for turbulent events (assumption #1 in the Introduction), using the DNS database. Young, preturbulent overturns are characterized by $R_{OT} < 1/2$. Shortly after transition, the ratio increases to order unity. As turbulence decays, R_{OT} increases further to values substantially greater than 1. These results are entirely consistent with the conclusions of Wijesekera and Dillon (1997), which were derived from observational data by using entropy as a time measure. A convenient alternative expression of the time dependence shown in figure 2a is given by

$$t_N \equiv \int_{t_o}^t \frac{\hat{N}(t')}{2\pi} dt' = 0.2 + 3.2 \log_{10} R_{OT} \pm 0.5, \quad (2)$$

which produces an estimate of the time, in buoyancy periods, since the maximum R_b was reached (at t_o , shortly after the transition to turbulence). The estimate is also valid when $t_N < 0$, i.e. for preturbulent overturns. The error estimate 0.5 pertains to the DNS case #1 ($Pr = 7$). The uncertainty will be larger if this formula is applied in more general situations.

6. Γ_d as a surrogate for the flux coefficient

We now test the second of the two assumptions described in section 2. This requires assessing the usefulness of Γ_d as a surrogate for Γ_i . For this calculation, the DNS data is altered in two ways to facilitate comparison with observational results: a weak, random noise field is added to ϵ , and profiles for which $\epsilon < 4 \times 10^{-10} m^2 s^{-2}$ are discarded. The flux coefficient is then computed as $\Gamma_d = \kappa CN^2/\epsilon$. The evolution of Γ_d is shown in figure 2b. To assess the effect of noise, we also show Γ'_d , which is calculated from the untreated ϵ fields. Γ'_d and Γ_i follow similar evolutionary patterns, the main differences being $\Gamma'_d > \Gamma_i$ during the preturbulent phase and the tendency of Γ'_d to increase during the final stages of turbulence decay. The large discrepancy found in the preturbulent phase is not surprising, as the assumptions inherent in the Osborn-Cox formulation are invalid during this phase. The increase observed late in the simulation is related to the inaccuracy of the isotropic approximation of ϵ in this very weak turbulence (Smyth and Moum, 2000a). Nevertheless, the correspondence is reasonable while turbulence is strong, and even prior to transition Γ_d gives a qualitative indication of the large flux coefficient that characterizes that early phase.

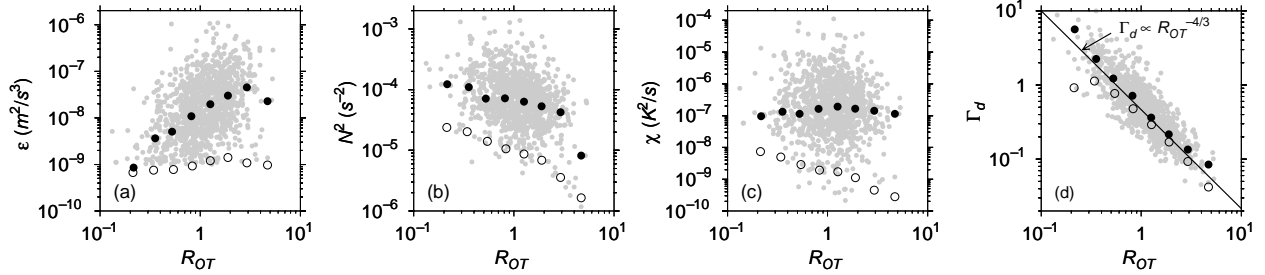


Figure 3: Γ_d and related quantities as functions of the length scale ratio $R_{OT} = L_O/L_T$, for turbulent overturns observed in TIWE and FLX91. (a) Volume-averaged perturbation kinetic energy dissipation rate. (b) Squared Brunt-Vaisala frequency. (c) Temperature variance dissipation rate. (d) Γ_d . The ordinate is interpreted as a surrogate for time. Shaded circles represent individual turbulent events from TIWE. Symbols represent bin averages taken over appropriate ranges of R_{OT} . Open circles (bullets) correspond to the FLX91 (TIWE) cruise.

Both the addition of the noise field and the acceptance criterion result in larger mean values of ϵ , and thus values of Γ_d that are smaller than Γ_d' . The result is improved agreement with Γ_i in the preturbulent phase, although this improvement is unrelated to the flow physics. After transition, the increase in apparent dissipation rates leads to underestimates of Γ_i . Unlike both Γ_i and Γ_d' , Γ_d does not asymptote to 0.2, but rather continues to decrease. We will see that this behavior is evident in the observational data also.

7. “Evolution” of Γ_d in observations

We have now assessed the validity of the two assumptions needed in the interpretation of the observational data. Accordingly, we next examine the relationship between Γ_d and R_{OT} in the microstructure data, interpreting the results in terms of the time evolution of the flux coefficient. The plotted points in figure 3 represent bin averages of the TIWE and FLX91 data with respect to R_{OT} . In the background, we show the individual events from which the bin averages were derived (for clarity, individual observations are shown for TIWE only).

For each dataset, the “evolution” shown in figure 3 corresponds qualitatively to our expectations. The TIWE results are generally more energetic than their counterparts from FLX91, mainly because of the strong background shear of the Equatorial Undercurrent. In each case, the dissipation rate ϵ grows initially, then decays. The bulk stratification N^2 decreases monotonically, as one would expect in an entraining turbulent layer. The scalar variance dissipation rate χ remains approximately constant in time for the TIWE data, while decreasing for the FLX91 data. This is consistent with our finding that preturbulent overturns generate strong temperature gradients and thus large χ (Smyth et al., 2000).

Unlike the quantities discussed previously, Γ_d shows considerable uniformity between the TIWE and FLX91 cases. In each case, Γ_d decreases monotonically over most of the evolution. Results for early times are likely to be influenced by the nonstationarity and inhomogeneity, both of which degrade the validity of the Osborn-Cox formulation. There is no indication of the asymptotic approach to a value near 0.2 as seen in figure 2b. Instead, the evolution of Γ_d exhibits an approximate power law behavior, with slope near $-4/3$, in both the FLX91 and TIWE datasets. This apparent discrepancy at late times is consistent with the result from DNS calculations shown in figure 2b, where we saw how the noise threshold decreases the apparent value of Γ_d when turbulence is weak.

8. Conclusions

We have employed a combination of numerical and observational methods to investigate mixing as it evolves over the lifetime of a turbulent overturn. The DNS data enable us to test assumptions that are needed for the interpretation of the observations, while the observational data allow access to realistic parameter

regimes that present-day computers cannot simulate. First, we assessed the dependence of Γ_i on time in the simulated flows. Second we used the simulated flows to test the usefulness of R_{OT} as a surrogate for time, and of Γ_d as a surrogate for Γ_i (assumptions 1 and 2 of the Introduction). Based on these results, we examined the dependence of Γ_d on R_{OT} using the observational data, and compared the results with expectations based on the time dependence of Γ_i in the simulations.

The result of these analyses is a self consistent picture, supported by both model and observations, in which the flux coefficient decreases dramatically over the lifetime of a turbulent overturn. For application to observations, this evolution may be parameterized as $\Gamma_i = 0.33 R_{OT}^{-0.63}$ (Smyth et al., 2000). The preturbulent phase (in which mixing is highly efficient) may be of secondary importance in circumstances where turbulence persists over long times, such as the Equatorial Undercurrent. In other cases, however, turbulence-driving shear is likely to be more intermittent, with the result that the initial stage of billow development contributes a more significant fraction of the net mixing.

Acknowledgements: This research was funded by the National Science Foundation. Computations were performed at Oregon State University's Environmental Computing Center.

References

- Gargett, A. and J. Moum, 1995: Mixing efficiencies in turbulent tidal fronts: results from direct and indirect measurements of density flux. *J. Phys. Oceanogr.*, **25**, 2583–2608.
- Hebert, D. and J. Moum, 1994: Decay of a near-inertial wave. *J. Phys. Oceanogr.*, **24**, 2334–2351.
- Lien, R.-C., D. Caldwell, M. Gregg, and J. Moum, 1995: Turbulence variability at the equator in the central pacific at the beginning of the 1991-1993 El Nino. *J. Geophys. Res.*, **100**(C4), 6881–6898.
- Moum, J., 1996a: Efficiency of mixing in the main thermocline. *J. Geophys. Res.*, **101**(C5), 12,057–12,069.
- Moum, J., 1996b: Energy-containing scales of turbulence in the ocean thermocline. *J. Geophys. Res.*, **101**(C6), 14095–14109.
- Oakey, N., 1982: Determination of the rate of dissipation of turbulent energy from simultaneous temperature and velocity shear microstructure measurements. *J. Phys. Oceanogr.*, **12**, 256–271.
- Osborn, T. R. and C. S. Cox, 1972: Oceanic fine structure. *Geophys. Fluid Dyn.*, **3**, 321–345.
- Ruddick, B., D. Walsh, and N. Oakey, 1997: Variations in apparent mixing efficiency in the North Atlantic Central Water. *J. Phys. Oceanogr.*, **27**, 2589–2605.
- Smyth, W., 1999: Dissipation range geometry and scalar spectra in sheared, stratified turbulence. *J. Fluid Mech.*, **401**, 209–242.
- Smyth, W., D. Hebert, and J. Moum, 1996: Local ocean response to a multiphase westerly windburst. part 2: Thermal and freshwater responses. *J. Geophys. Res.*, **101**, 22495–22512.
- Smyth, W. and J. Moum, 2000a: Anisotropy of turbulence in stably stratified mixing layers. *Phys. Fluids*, (in press).
- Smyth, W. and J. Moum, 2000b: Length scales of turbulence in stably stratified mixing layers. *Phys. Fluids*, (in press).
- Smyth, W., J. Moum, and D. Caldwell, 2000: The efficiency of mixing in turbulent patches: inferences from direct simulations and microstructure observations. *J. Phys. Oceanogr.*, (submitted).
- Wijesekera, H. and T. Dillon, 1997: Shannon entropy as an indicator of age for turbulent overturns in the oceanic thermocline. *J. Geophys. Res.*, **102**(C2), 3279–3291.
- Winters, K., P. Lombard, J. Riley, and E. A. D'Asaro, 1995: Available potential energy and mixing in density-stratified fluids. *J. Fluid Mech.*, **289**, 115–128.